The synthesis and thermoelectric properties of the Gadolinium-doped $Ge_xPb_{1-x}Te$ material

Bachelor thesis

Author: Yuqin Cui
Student number: s3215040
Supervisor: Dr. Graeme R. Blake
Second assessor: Dr. B. Noheda Pinuaga
Daily supervisor: Hong Lian
Date: 03-07-2018

Abstract

TE materials attracted a lot of attention during the last three decades due to their abilities to convert heat directly to electricity. There are several popular TE materials reported these years, including PbTe, GeTe, LAST and TAGS. Among these, the PbTe-GeTe alloy with different ratios was developed these years. However, with relatively high Seebeck coefficient and electrical conductivity, the thermal conductivities of PbTe-GeTe alloy are also pretty high (around 2.5 $Wm^{-1}K^{-1}$). Thus, an extra element was doped in the binary system. In this bachelor thesis, the $Ge_xPb_{1-x}Te$ based materials doped by 2% gadolinium with two different sites (cation and anion) and different synthesis methods were investigated to improve the thermoelectric properties by reducing thermal conductivity while maintaining the other factor.

The result showed that the thermal conductivity of all samples reduced at least 2 times compared to the reference one.

The optimized and stable sample was Gd-doped in anion site with excess Ge and via air-cooling method, showing the lowest thermal conductivity around 0.4 $Wm^{-1}K^{-1}$ in third cycle measurement.

Table of Contents

Introduction

Thermoelectric materials, which can generate electricity from waste heat directly, or be used as solid-state Peltier coolers have received great attention recently due to their properties. This is mainly because of the need for cryo-coolers for electronic devices, increasing environmental awareness in the generation of electricity, and potential applications in low noise refrigeration. [1]
When a temperature gradient is formed within a thermoelectric semiconductor, the charge carriers will diffuse from the hotter side to the colder side then generate an electrical voltage. Contrarily, when an electrical voltage is applied to a thermoelectric material, it will produce a temperature gradient, which can be used for heating or cooling.
The performance of a thermoelectric material is defined by some interrelated material properties and the aim of the current research is to optimize the combination of these properties. [2] To evaluate the ability of thermoelectric materials with respect to energy conversion, a metric called the thermoelectric materials figure of merit $\mathrm{ZT} = \frac{S^2\sigma}{\kappa}T$ is well-defined, where S is the Seebeck coefficient, σ is the electrical resistivity, κ is the thermal conductivity and T is the absolute temperature of the material at a certain point. In the other word, ZT depends on S(T), σ (T), and κ(T). [2]
The value of ZT for current thermoelectric materials lies near unity. Some materials reach 1.8 or higher, so the aim is to raise the ZT value above 2. During the past 10 years, significant development in reducing the lattice thermal conductivity has been made to reduce κ(T), which is the thermal conductivity. However, some materials have reached the amorphous limit, meaning that little further improvement in ZT can be expected by reducing thermal conductivity. Thus, the electronic part of the figure of merit, more specifically, the Seebeck coefficient and resistivity, has attracted more attention recently.
A theoretical way to enhance the Seebeck coefficient is by a controlled distortion of the electronic density of states, and there are some successful attempts to do this in the literature.

Ge-Pb-Te based materials have been one of the most popular thermoelectric materials. These materials are derived from pristine GeTe which is not a suitable thermoelectric material because of the high carrier concentration due to its intrinsic Ge vacancies. The optimized properties can be reached by adding donor dopants to reduce the hole concentration.
For example, GeTe was alloyed with PbTe to optimize the TE properties in terms of increasing the Seebeck coefficient and decreasing the thermal conductivity. Different alloy ratios of $Ge_xPb_{1-x}Te$ have been studied, allowing ZT values above 1 to be reached.
Doping with lanthanides has been reported to give rise to the presence of quasi-local impurity states in the electronic band structure of samples, which stabilizes the Fermi level and creates additional resonant electron scattering, which results in the increase of the Seebeck coefficient. [4] In this bachelor thesis, the improvement of the thermoelectric properties of the $Ge_{0.51}Pb_{0.49}Te$ system by doping with Gd via three different methods is reported. Chapter 1, chapter 2 and chapter 3 describe an overview of the thermoelectric effect, a literature review of the Ge-Pb-Te system and the lab instruments used, respectively, while chapter 4 and chapter 5 report the experiments, results and discussion.

Chapter 1. Thermoelectricity

Thermoelectricity is a phenomenon that can convert heat into electricity and vice versa. The "thermoelectric effect" can be subdivided into three effects, which are the Peltier effect, Seebeck effect and Joule-Thomson effect. In 1821, a German physicist Thomas Seebeck observed that when two dissimilar metals were connected to each other and a temperature gradient was applied, then there would appear a voltage difference proportional to the temperature gradient. The Seebeck coefficient was then defined as the ratio of the voltage gradient and temperature difference ($S = \frac{\Delta V}{\Delta T}$), which is related to the intrinsic properties of the materials.

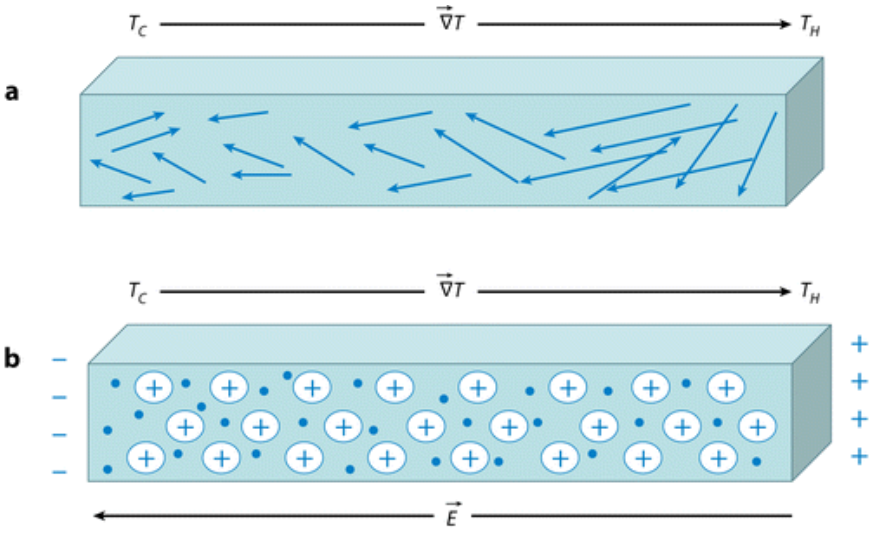

Tritt TM. 2011.
Annu. Rev. Mater. Res. 41:433–48

Figure 1.1. A description of thermoelectric effect under the external temperature gradient [3]

After a few years, Jean Charles Athanase Peltier discovered the inverse of the Seebeck effect, where an electrical current passed through the junction of two dissimilar materials can absorb or generate heat depending on the direction of the current, which is called the Peltier effect. The conversion efficiency of TE materials, which relies on the Carnot efficiency ($^{\Delta T}/_{T_H}$) and the figure of merit ZT, which evaluates the performance, is given below:

$$\eta = \frac{T_H - T_C}{T_H} \frac{\sqrt{1 + ZT_{avg.}} - 1}{\sqrt{1 + ZT_{avg.}} + \frac{T_C}{T_H}} \quad \text{(eq 2.1)}$$

where T_H is the temperature of the hot end, T_C is the temperature of the cold end and $T_{avg.}$ is the average temperature.
The thermoelectric figure of merit $ZT_{avg.}$ is determined as follows:

$$ZT = \frac{S^2\sigma}{\kappa} T \quad \text{(eq 2.2)}$$

From equation 2.1, it can be determined that the optimized performance of a TE material has to fulfil the following criteria: high Seebeck coefficient, high electrical conductivity and low thermal conductivity. These properties rely on the inter-related parameters of the material.

1.1 Selection of suitable TE materials: carrier concentration engineering

To get a high Seebeck coefficient, the charge carriers of a TE material should only be one type, either p-type or n-type. Otherwise, both kinds of charge carriers would move to the cold end and cancel out the Seebeck voltage. The Seebeck coefficient is defined as equation 2.1.1 for degenerate semiconductors and metals: [5]

$$S = \frac{8\pi^2 k_B^2}{3eh^2} m^* T \left(\frac{\pi}{3n}\right)^{2/3} \text{ (eq 1.1.1)}$$

where k_B is the Boltzmann constant, e is the charge of an electron, h is Planck's constant, m* is the effective mass of the carriers and n is the carrier concentration.

From eq 2.1.1, it can be concluded that insulators with low carrier density or semiconductors would have high Seebeck coefficients. However, low carrier density also leads to low electrical conductivity, shown as follows: [5]

$$1/\rho = \sigma = ne\mu \text{ (eq 1.1.2)}$$

where ρ is electrical resistivity, σ is electrical conductivity, n is the concentration of charge carriers, e is the charge of an electron and μ is the mobility.

The thermal conductivity can be divided into two parts:

$$\kappa = \kappa_e + \kappa_l$$

where κ_e and κ_l are the electronic and lattice thermal conductivity respectively. κ_e is difficult to decrease due to its positive correlation with the electrical conductivity:

$$\kappa_e = L\sigma T = ne\mu LT$$

where L is the Lorentz factor, which is constant (2.4×10^{-8}) for metals and degenerated semiconductors, but varies when the carrier concentration is lowered.

Therefore, the optimized TE material should have low κ_l. Lattice thermal conductivity in a semiconductor is given by

$$\kappa_l = \frac{1}{3} C_v V_s \lambda_{ph}$$

where C_v is the heat capacity, V_s is the velocity of sound and λ_{ph} is the mean free path of the phonons.

The first criterion to select a suitable thermoelectric material is the carrier concentration, which should usually be around 10^{19}-10^{20} cm^{-1} for optimizing all three parameters (κ, S and σ).

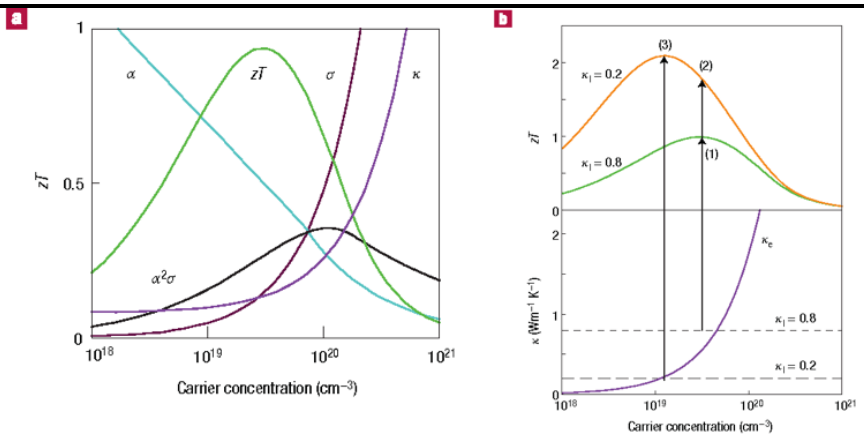

Figure 1.1.1 Optimized zT through carrier concentration tuning [5]

1.2 Methods to improve thermoelectric figure of merit

A common strategy to achieve a high figure of merit consists of two parts: increasing the power factor, and decreasing the thermal conductivity. In this section, developments over recent decades are discussed.
Previous research reported the dimensionless merit factor (β) of thermoelectric materials can be separated as follows: [7]

$$\beta = 9\frac{U}{\kappa_{lat}}\left(\frac{T}{300}\right)^{\frac{5}{2}}$$

where U is the weighted mobility (a measure of the electrical properties), which is derived as

$$U = (m^*)^{3/2}\mu$$

where m* is the carrier effective mass (the free electron mass) and μ is the mobility. m* relates to m_b*, which is the band effective mass, expressed as follows:

$$m^* = (N_V)^{2/3} m_b^*$$

where N_V is the number of equivalent degenerate valleys of the band structure.
From all the considerations above, N_V, m_b*, μ should be maximized and κ_{lat} should be minimized at a constant n (carrier concentration, described in section 1.1). [7]

1.2.1 Enhancement of carrier effective mass

Increasing the number of band extrema N_V
The number of band extrema is influenced by the crystal symmetry. This is large when the crystal structure is symmetric. The N_V of lead telluride, which has a cubic rocksalt structure, is 4 and 12 at the L and Σ points of the valence band, respectively.
An attempt to increase N_V was recently carried out on tetragonal chalcopyrite compounds to achieve a lower energy-splitting parameter (or large N_V).
Another promising approach is to converge different bands in the Brillouin zone to within a few k_BT of each other in energy. Taking lead chalcogenides as an example, there are two valence bands: the one at the L point has an N_V of 4 and the other at the Σ point of the Brillouin zone has a much larger N_V of 12. In the general case, the energy difference of these two bands is large enough to separate the bands and make the Σ band irrelevant to charge transport. However, the difference between the two bands ($\Delta E_{L-\Sigma}$) can be significantly reduced via alloying with other elements (e.g. Mg, Cd, Sr or Mn in PbTe), thus making the two bands converge gradually, while the effective N_V is enlarged to 12 and better thermoelectric performance is shown.

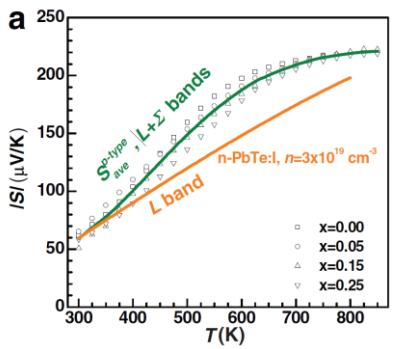

Figure 1.2.1.1 The existence of the second (heavy Σ) valence band below the principal (light L) valence band in PbTe leads to high Seebeck coefiecient. [8]

Increasing carrier effective mass m_b^*

The carrier effective mass in a band is related to the bending of the bands and can be adjusted via distorting the bands, which increases the density of states in the vicinity of the Fermi level.

Chemical doping can enhance m_b^* by band flattening and resonant levels. However, the increasing of m_b^* will lead to a decrease in carrier mobility and electrical conductivity. Adoption of dopants containing highly localized orbitals which can decrease orbital overlap can achieve band flattening effects. For example, using La to substitute Sr significantly flattens the conduction band of SrTiO3 perovskites and significantly increases the density of states effective mass of the electrons, thereby leading to higher power factors and thermoelectric figures of merit. Band flattening not only increases m_b^*,but also enlarges the band gap E_g according to the Kane-band model, which can suppress the detrimental effect of bipolar diffusion on the TE properties. This relationship is shown below:

$$\frac{\hbar^2 k^2}{2m_b^*} = E(1 + \frac{E}{E_g})$$

Here $\hbar$ is the reduced Plank's constant, k is the crystal momentum, and E is the energy of the states.

Resonant levels (RLs), which were firstly proposed in metals, originate from the coupling between the electrons of a dilute impurity with those of the conduction or the valence band of the host solid. The classical case is a donor impurity in a semiconductor, such as P in Si shown below. [7]

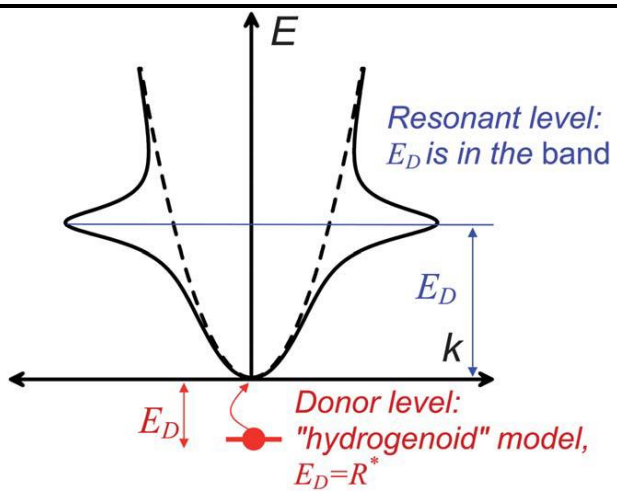

Figure 1.2.1.2 Schematic representation of a conduction band, a hydrogenoid impurity, and a resonant impurity. [19]

RLs create an excess density of states (DOS) near the resonant energy and can give rise to improved m_b^* and thus enhanced Seebeck coefficients if there is excess DOS at the energy corresponding to the resonant level. [19]

The application of resonant impurities has been used in electrical power generation (such as thallium in the valence band of PbTe) and Peltier cooling (such as tin in the valence band of Bi_2Te_3). [19]

1.2.2 Improvement of carrier mobility

Most TE materials have carrier concentrations of the order of 10^{19}–10^{21} cm^{-3}, which is the optimized range of n values for high ZT. (Figure 1.1.1 a)
However, for heavily doped semiconductors, the carrier mobility decreases because of increased ionized impurity scattering due to the high concentration of the carriers when compared to lightly doped materials.

1.2.3 Reduce lattice thermal conductivity

During the last decades, the classical approach scientists have used is to reduce the lattice thermal conductivity. Glass shows the lowest lattice thermal conductivity due to its disordered structure which does not allow rapid transport by phonons. The thermal conductivity of a glass is regarded as the conceptual minimum thermal conductivity, κ_{min}. However, glasses are not good TE materials due to the lack of 'electron-crystal' properties. They have lower mobility because of increased electron scattering and lower effective masses because of broader bands. [5] Thus, the 'phonon-glass electron-crystal' concept of TE materials was proposed by Slack [6], where the ideal material has the lattice thermal conductivity of a glass with high charge carrier mobility.
Phonon waves can be scattered at crystal defects like dislocations, interfaces, point defects etc., which introduce additional thermal resistance and give a reduction of κ_{lat}.
There are two common methods to reduce lattice thermal conductivity. A short description of these is given below. [5]

Atomic Scale: Synergistic Alloying.
The first approach to decreasing the lattice thermal conductivity is the introduction of lattice imperfections in the main lattice via doping or alloying. In 1959 and 1960, Klemens [12] and Callaway [11] [10] reported that the reduction of κ_{lat} could be achieved by a combination of strain field fluctuation and mass contrast.
The scattering parameter which describes the degree of reduction was proposed by Abeles below [13]:

$$\Gamma = x(1-x)[\left(\frac{\Delta m}{m}\right)^2 + \varepsilon(\frac{a_{disorder} - a_{pure}}{a_{pure}})^2]$$

where x is the fraction of doping, $\Delta m/m$ is the change of atomic mass, $a_{disorder}$ and a_{pure} are the lattice constants of disordered and pure alloys respectively, and ε is an elastic property-related adjustment parameter. [9]
From the equation above, it can be concluded that a higher doping fraction, a larger mass difference between the dopant and host element, which creates disorder in lattice, and a lattice mismatch between the disordered and pure phases can give a maximum Γ, thus minimum κ_{lat}.

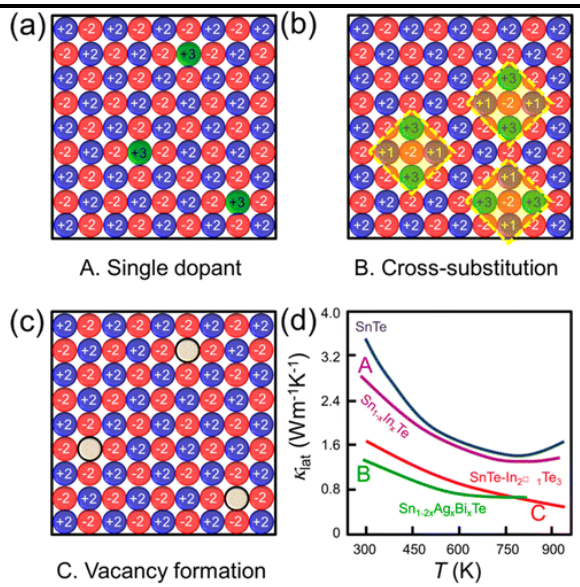

Figure 1.2.3.1 Schematic representation of various types of point defects [9]

Three different doping approaches are shown in Figure 1.2.3.1:

- Single-element doping
- Cross-substition
- Formation of lattice vacancies

Nanoscale: nanostructuring with second phases

Defects in crystals lead to the scattering of phonons with nanometer scale wavelengths. The geometric length of the defects should be small, around several nanometers. Moreover, the nanostructures should be distributed to give maximal interface density over a large volume. An example of this method is the presence of SrTe nanoscale precipitates in the PbTe matrix. [9] The second phase (SrTe) is homogeneously dispersed in the host material of PbTe.

In addition to the two important methods described above, some other methods have been developed recently to reduce thermal conductivity, including ***mesoscale structuring***, ***structural complexity in zintl phases*** and the ***introduction of super-lattices.*** [7]

Chapter 2. Ge-Pb-Te System: A Literature Review

This chapter will provide an overview of thermoelectric materials based on the Ge-Pb-Te system, including microstructure, phase diagram and thermal properties. The influence of different chemical compositions or ratios of Ge and Pb will also be discussed.

2.1 GeTe and PbTe thermoelectric materials

Lead Telluride (PbTe) was one of the first materials investigated as a thermoelectric. However, it has recently been revealed to be much better than earlier believed. The crystal structure of PbTe has Fm3m symmetry and is of rock salt type. X-ray diffraction studies show that the lattice constant of PbTe is 6.46 Å and the material density is 8.25 g/cm^3 with a melting temperature of 923 ℃ for intrinsic PbTe. Due to naturally occurring Pb vacancies, intrinsic PbTe is always p-type. Some approaches for optimizing the properties of intrinsic PbTe have been developed in recent years, such as nanostructured PbTe systems. However, the pure PbTe was tried to be avoided in application because of its toxic nature. [17]

Germanium Telluride (GeTe) have been used for thermoelectric applications since the 1960's. Germanium telluride is a narrow band gap p-type semiconductor.
GeTe exhibits a very high carrier concentration which is around 10^{21} cm^{-3} due to a large number of Ge vacancies in its crystal structure and results in high electrical conductivity. GeTe experiences a second-order phase transition from the low-temperature rhombohedral (R3m) to the high-temperature cubic ($Fm\bar{3}m$) structure at ~700 K. [16]For thermoelectric properties, GeTe shows a Seebeck coefficient value of 34 μV K^{-1} at room temperature and 8 Wm^{-1}K^{-1} of thermal conductivity, caused by the high p-type carrier concentration. To enhance the performance of GeTe, a rock-salt component like AgSbTe2, SnTe, and PbTe can be alloyed with GeTe.

2.2 PbTe–GeTe alloys & Doping motivation

Recently, $Ge_xPb_{1-x}Te$ have been reported to increasing Seebeck coefficient of Pristine GeTe using the donor dopant nature of Pb at the ratio x = 0.87. However, although the thermal conductivity of $Ge_{0.87}Pb_{0.13}Te$ was also reduced to 4 Wm^{-1}K^{-1}, which is 2 times smaller than pristine GeTe, it's still not comparable with TAGS-85, whose thermal conductivity is below to 1 Wm^{-1}K^{-1}. Thus, the further investigation was made to minimize thermal conductivity by varying the ratio using phase diagram as well as adding a doping elements or substituent a certain element.
The phase diagram of the PbTe-GeTe quasi-binary system shown in Figure 2.2.1 is important to understand the direction of research on PbTe–GeTe alloys.

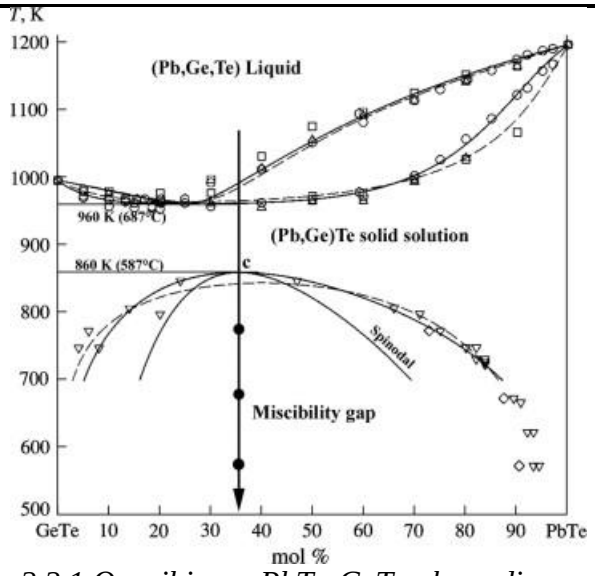

Figure 2.2.1 Quasibinary PbTe-GeTe phase diagram [21]

The diagram depicts a spinodal decomposition, which can be used to develop a fine two-phase mixture via the decomposition of the super-saturated solid solution. [21] Gorsse *et al*. reported a series of samples with ratio $Pb_{0.36}Ge_{0.64}Te$, which have the low thermal diffusivity using spinodal decomposition. [21]

Doping with Bi_2Te_3

In 2014, Bi_2Te_3 was introduced as a donor dopant in $Pb_{0.13}Ge_{0.87}Te$ and caused a improvement of thermoelectric properties of the original material. [23] From their research, Bi_2Te_3 not only reduces the thermal conductivity through point-defect scattering by enhancing the PbTe solubility in GeTe and also increase Seebeck coefficient by medication of the relative energy of the light (L) and heavy valence bands (Σ). [23]

Substituent Te with Sn

Another method to enhance the TE properties are using another element to substituent Te. $Ge_{0.55}Pb_{0.45}Te$, which was the best ratio using spinodal decomposition in theory, was substituted with Se in anion site. The present of Se was found to promote the solid solubility of Pb in Ge-rich phase and hence scattering on phonons transport, leading to low thermal conductivity. [22]

Chapter 3. Material and Method

This section will cover the methods used and the characterization of Gd-doped GePbTe-based thermoelectric materials. A short introduction to the characterization techniques will be given. The techniques we used in our experiments included XRD (X-ray Diffraction), SEM (Scanning electron microscopy), Seebeck coefficient measurement and thermal conductivity measurement.

Element Name	Purity	Company
Ge	99.9%	Alfa Aesar
Gd	99.9%	Alfa Aesar
Te	99.9%	Alfa Aesar
Pb	99.9%	Alfa Aesar

Table 3.1 Information on the elements used in sysnthesis

3.1 Experimental Section

In this section, the synthesis method will be described.

The alloys of $Ge_{0.51}Pb_{0.49}Te$ doped with gadolinium were prepared by a solid state method by directly reacting the constituent elements, Ge, Pb, Te and Gd. Pure elements were carefully weighed and then fully mixed by grinding with a mortar and pestle for at least 10 minutes. After that, the mixture was placed in a quartz ampule, then evacuated and sealed. The sealed quartz ampule was then placed in a tubular furnace and heated to 850℃ within 1 hour. The ampule was kept at that temperature for a certain time and rotated every 10 minutes in order to ensure homogeneity. During this procedure, the elements undergo a chemical reaction to form an alloy. Some of the samples underwent an annealing stage where the temperature was deceased to 650℃ and kept for at least 3 hours while others were cooled directly from the melt. Finally, the melts were quenched in water or air-cooled to room temperature.

Solidified shiny ingots with approximately rectangular shape were obtained and then sliced with a diamond wire saw followed by polishing with sandpaper and ethanol to obtain flat and uniform rectangular pieces for high temperature thermoelectric measurements. Two small pieces were cut from each ingot; one was powdered for X-ray diffraction and the other was used to prepare an SEM sample to examine the micro-structure.

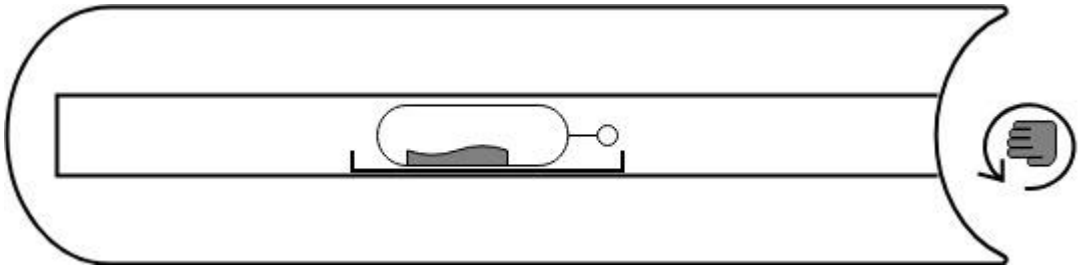

Figure 3.1.1. Schematic picture of furnace and sealed quartz tube

3.2 X-ray powder diffraction

X-ray powder diffraction is a powerful technique used to do phase analysis and to study the crystallographic properties of the samples. In our laboratory, a Bruker D8 Advance X-ray diffractometer was used to test all the samples at room temperature. The X-ray diffractometer generates an X-ray beam in a sealed X-ray tube by hitting a copper anode with a high energy beam of electrons. A tungsten filament is used as the electron source.
The electrons then are accelerated to the anode by applying a 40kV field and leads to a spectrum comprised of a bremsstrahlung background on which X-ray emission lines characteristic of the metal target are superimposed. During this thesis, we used a Cu anode.

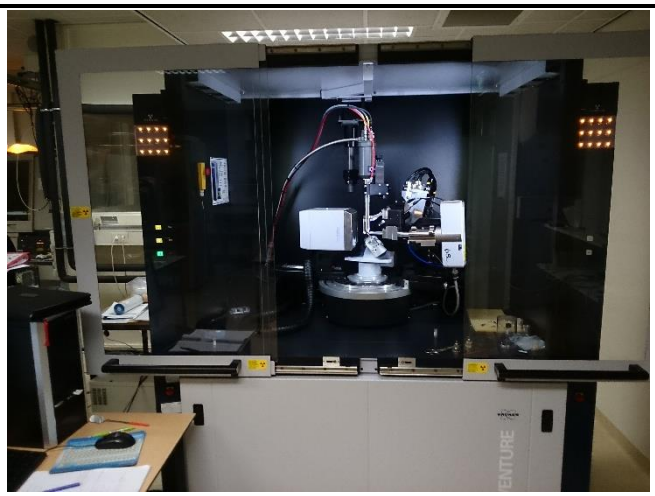

Figure 3.2.1 picture of Bruker D8 advanced X-ray diffractometer in our lab

The samples were scanned over a range of 2θ = 20 degrees to 80 degrees. The samples were scanned for long time (14 hours) to decrease the background noise and to check for impurity phases.

3.3 Seebeck coefficient and resistivity measurement

The Seebeck coefficients and electrical conductivity were measured at high temperature using a Linseis LSR-3 setup. This machine is designed to measure the Seebeck coefficient and resistivity with increasing temperature in the range 300K to 1073K under helium atomosphere using automated data acquisition software. The temperature dependent Seebeck coefficient and electrical conductivity can be measured on a sample with cylindrical or rectangular shape with dimensions of at least 7 mm.
The schematic of the machine is shown in Figure 3.2.1:

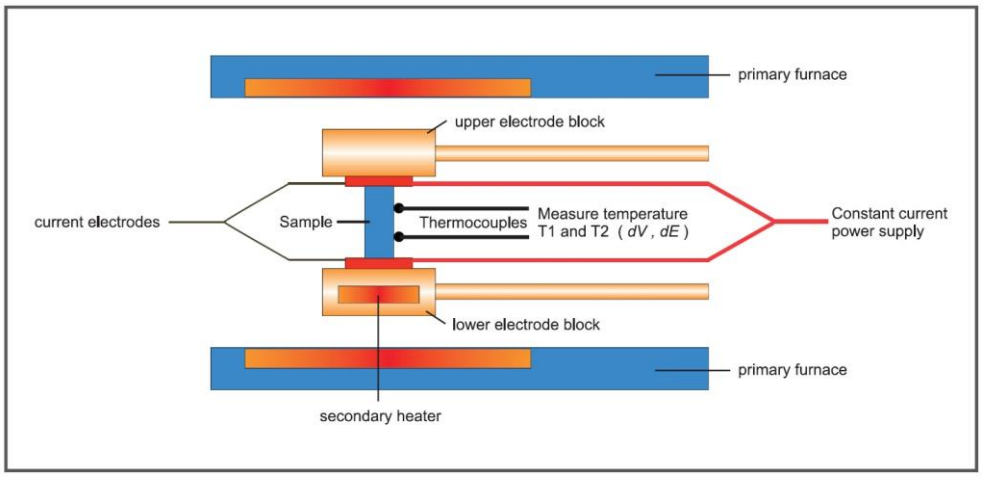

Figure 3.3.1 The schematic layout of Linseis LSR-3 setup

In this thesis, the as-synthesized ingots were cut and polished to rectangular shapes and sandwiched vertically between two platinum electrode holders. There are two sources of heat in the machine. The primary furnace covers the entire measurement assembly and is used to heat the sample up to a specific temperature. The secondary heater is contained in the lower electrode block and is used to generate a temperature gradient across the sample once it has been heated and kept at the desired measurement temperature.
The Seebeck coefficient is then obtained by measuring the temperature gradient (ΔT) which is the difference between the upper and lower temperature T_1 and T_2 between the thermocouples attached to the sample (see figure 3.3.1), and the electromotive force, dE, generated from the same wires in response to the temperature gradient. The Seebeck coefficient is then automatically calculated as below, being dependent on the Seebeck voltage versus temperature difference at a constant average temperature:

$$S = \frac{\Delta V}{\Delta T} - S_{probe}$$

The electrical resistivity is determined using the DC 4-terminal method by applying a constant current and measuring the voltage different, dV, between the thermocouples connected to the sample after subtracting the thermo-electromotive force between the leads. The electrical resistivity is then calculated as follows:

$$\rho = \frac{RA}{l}$$

where A is the area of the sample and l is the distance between the probe thermocouples.

3.4 Thermal conductivity measurement

Thermal conductivity is one of the important parameters in the thermoelectric figure of merit. It describes the ability of a material to conduct heat. In this project, thermal conductivity was calculated from the thermal diffusivity as follows:

$$\kappa = \rho C_p D$$

Here ρ is the sample density, C_p is the specific heat capacity and D is the thermal diffusivity. Thermal diffusivity can be calculated from the thickness of the sample and the time needed for it to reach half of the maximum temperature while heating is induced by a laser flash. The method used in this project is the laser flash technique with a Linseis LFA 1000 apparatus.

The density of the samples was calculated by measuring their weight and dimensions, and the heat capacity was estimated by the Dulong-Petit approximation:

$$C_p = \frac{3R}{M}$$

where R is the universal gas constant and M is the relative molecular mass.

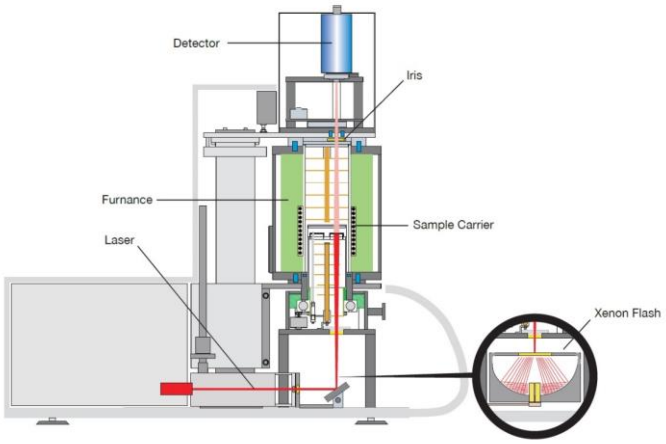

Figure 3.4.1 The Linseis LFA 1000 setup

3.5 Scanning electron microscopy (SEM) and energy dispersive X-ray(EDS)

Scanning electron microscopy (SEM) with a secondary electron detector is a technique used to visualize crystal shape and reveal the surface morphology of the sample by giving images with three-dimensional appearance. The signals used by the SEM to produce images are from interactions of the electron beam with atoms at different depths within the sample.
Several different types of signals are produced, which are secondary electrons, reflected or back-scattered electrons, and characteristic X-rays.
An EDS analysis with SEM can be used to do quantity measurement for different elements in the sample.

Chapter 4. Results and Discussion

In this chapter, the micro-structure and thermoelectric properties of 5 Gd-doped materials with different doping positions, cooling methods and holding times were discussed and compared with each other or with literature values. The solid state reaction method described in chapter 4 was applied to synthesize all alloys.
Below showed the information of all the sample.
Sample 1 - Gd for Te with 1 h reaction and quench: The nominal chemical formula sample 1 is $Ge_{0.49}Pb_{0.51}Te_{0.98}Gd_{0.02}$, suggesting that 2% Gd replaces Te on the anion site. The theoretical molecular weight is 266.7623 g/mol.
The synthesis method is described below: the quartz tube was heated to 850 ℃ at 14 ℃ /minute for about 1 hour, and the tube was kept at that temperature for 1 hour before it was quenched in cold water to room temperature (Figure 4.1.1 black line).
Sample 2 - Gd for Ge with 1 h reaction and quench: The nominal chemical formula sample 2 is $Ge_{0.49}Pb_{0.51}Te{\cdot}Gd_{0.02}Te_{0.03}$, suggesting that 2% Gd replaces Gd on the anion site, which was theoretically more favorable. The theoretical molecular weight is 273.1423g/mol.
The synthesis method is described below: the quartz tube was heated to 850 ℃ with 14 ℃ /minute for about 1hour, and the tube was kept at that temperature for 1 hours then quenched into cold water to room temperature. (Figure 4.1.1 black line).
Sample 3: Sample 3 was made to reproduce sample 1 and had the same properties.
Sample 4 - Gd for Te with 1 h reaction and air-cooling: The nominal chemical formula sample 4 is $Ge_{0.49}Pb_{0.51}Te_{0.98}Gd_{0.02}$.
The synthesis method is described below: the quartz tube was heated to 850 ℃ with 14 ℃ /minute for about 1 hour, and the quartz was kept at that temperature for 1 hours then quenched into cold water to room temperature. (Figure 4.1.1 red line).
Sample 5 - Gd for Te with 3 h reaction and quench: The nominal chemical formula sample 5 is $Ge_{0.49}Pb_{0.51}Te_{0.98}Gd_{0.02}$.
The synthesis method is described below: The synthesis method is described below: the quartz tube was heated to 850 ℃ with 14 ℃ /minute for about 1 hour, and the quartz was kept at that temperature for 3 hours then air-cooling for about 8 hours to 25 ℃. (Figure 4.1.1 red line).
Sample 6 - Gd for Ge with 3 h reaction and air-cooling: The nominal chemical formula sample 5 is $Ge_{0.49}Pb_{0.51}Te_{0.98}Gd_{0.02}$.
The synthesis method is described below: the quartz tube was heated to 850 ℃ with 14 ℃ /minute for about 1 hour, and the quartz was kept at that temperature for 1 hours then air-cooling for about 8 hours to 25 ℃. (Figure 4.1.1 blue line).

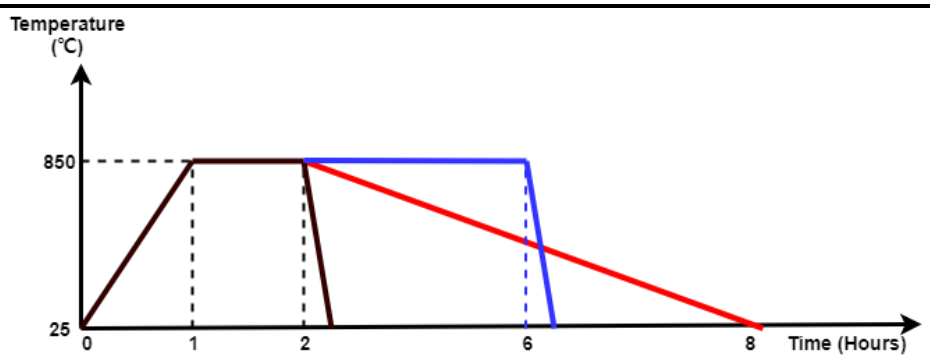

Figure 4.1.1 Synthesis method for all samples

4.1 Microstructure Analysis

The powder XRD of all the samples were measured at least for three hours and the software GSAS was used to refine the parameters and angles of different phases, below were the XRD patterns in one graph for all samples. The color of each line matched with synthesis methods above.

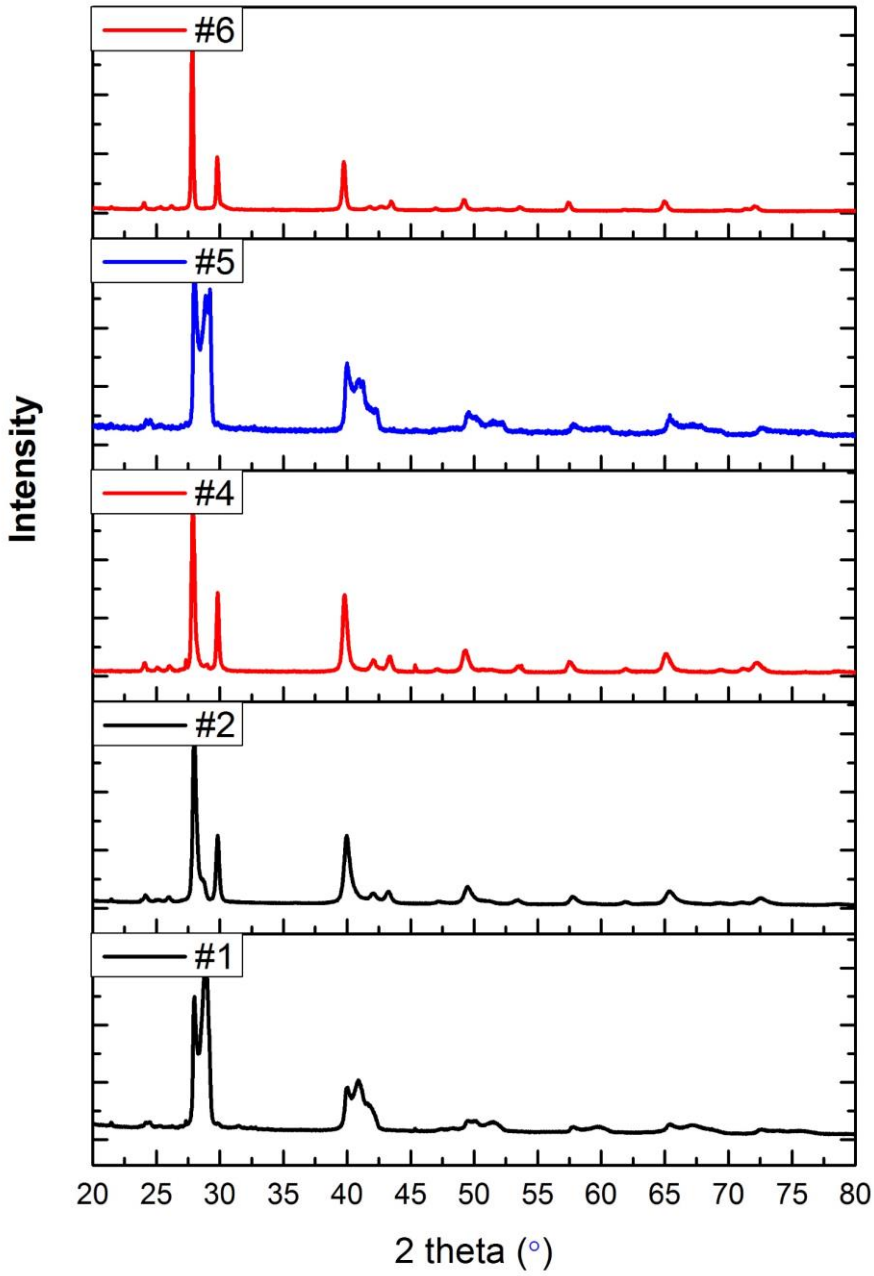

Figure 4.1.1 Powder XRD pattern for all samples, the color of line coordinated to the synthesis methods

Overall speaking, all five samples contained Pb-rich cubic phase and Ge-rich rhombohedra phase from GSAS refined XRD. However, the calculated XRD profiles of samples didn't fit the measured pattern perfectly, indicating that there were probably more phases (cubic and rhombohedral) that cover a range of lattice parameters. This hypothesis was supported by the SEM images, where the phase boundaries were poorly defined.

$Ge_{0.51}Pb_{0.49}Te+Gd$	sample 1	sample 2		sample 4	sample 5	
			GeTe-based phase			
space group				R3m		
sturcture type:				GeTe (Rhombohedra)		
parameter a	4.417(2)	4.3022(8)		4.305(6)	4.447(1)	4.411(1)
α	58.85(2)	58.24(1)		58.11(8)	58.83(2)	58.18(1)
phase fraction	0.84041	0.296(4)		0.377(4)	0.58368	0.20671
			PbTe-based phase			
space group				Fm-3m		
sturcture type:				NaCl (Cubic)		
parameter a	6.357(2)	6.382(5)	6.299(1)	6.404(5)	6.384(1)	
phase fraction	0.158(5)	0.54392	0.16033	0.61519	0.209(6)	
			Ge-phase			
space group				Fd-3m		
sturcture type:				Cubic		
parameter a	5.651(3)	-		5.6594	-	
phase fraction	0.00199	-		0.00802	-	
Rp	0.1108	0.0842		0.0783	0.0946	
wRp	0.1477	0.1191		0.1099	0.1260	

Table 4.1 Room temperature refined lattice parameter and phase fractions of sample 1, 2, 4 and 5

Effect of doping with Gd on the cation or anion site

In reality Gd is likely to occupy cation vacancy sites. However, the hypothesis was made that with a small amount of Gd (2%) in the certain chemical composition ($Ge_{0.49}Pb_{0.51}Te_{0.98}Gd_{0.02}$), Gd would be doped into Te site. Sample 1 & 2 and sample 4 &6 were performed in the same cooling method (quench) with different doped position. Powder XRD showed a big difference for these two groups of materials.

The first differences were the extra Ge peaks in Gd-anion site samples. For all of $Ge_{0.49}Pb_{0.51}Te_{0.98}Gd_{0.02}$ materials, there were always some Ge left, which can be distinguished from a small peak at around 2 theta = 46°, while there were no obviously Ge peaks in $Ge_{0.49}Pb_{0.51}Te{\cdot}Gd_{0.02}Te_{0.03}$, indicating that there was no Ge left for the designed experiments 2 and 6 (Gd on the anion site). The main non-stoichiometric influences are doubly ionized metal vacancies, Moreover, Ge nano-precipitates enhanced phonon scattering sufficiently, [22] which leads to the change of macro-properties.

The second difference was the peak width. In Gd-anion site samples, the peaks were more broaden than Gd-cation site one, showing that the doped Gd complicated microstructure more in Gd-anion site materials.

Last but not least, the XRD peaks coordinated to rhombohedra Ge-rich phase of sample 2 shifted a bit right compared to sample 1, indicating the changes of parameter and angle of Ge-rich GeTe rhombohedra phase.

To investigate further, SEM and EDS mapping were made for sample 1 and sample 2.

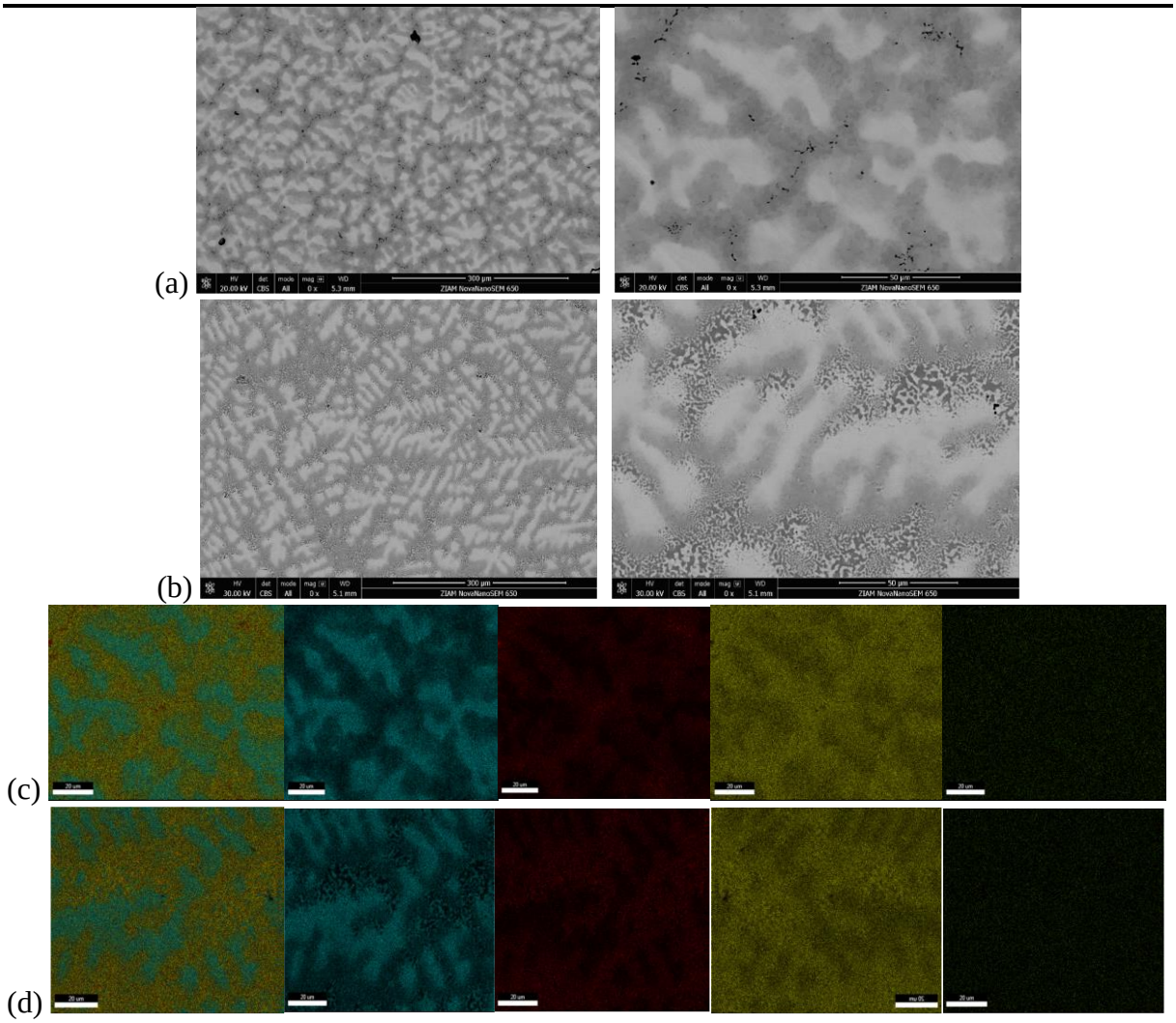

Figure 4.1.2 SEM images of sample 1 (a) and 2 (b), EDS mapping of sample 1 (c) and sample (d). The mapping elements were overall, Pb, Ge, Te and Gd from left to right.

From the SEM image, the main phases and grain sizes were similar. However, the phase boundaries of sample 2 were more clear than sample 1, coordinated the sharper XRD peaks. In EDS mapping image, the Gd was separated homogeneously in the sample, which means there were no Gd-rich precipitates in both samples.

Effect of quench versus slow cooling

Different cooling methods gave a large change of microstructure for Gd on anion site samples, the air cooling method leaded to wider peaks and the right shift of rhombohedra peaks. However, for Gd on cation sit samples, the microstructures of the samples undergo both cooling methods were similar, the only difference of sample 6 was the disappearance of another distinguished cubic phase with small phase fraction compared to sample 2. From figure 4.1.2 (a) and (b), the sample 1&2, which quenched from the melt consists of Ge-rich phase formed with dendrites of Pb-rich phase.

The reason of these phenomenon can be explained by the fact that slow cooling process would introduce the inhomogeneous microstructure because that made the materials crossed the miscibility gap under 800K while quench method maintained the structures of sample in liquid phase temperature. Also, the excess Ge in sample 1 gave more complexities in

microstructure than sample 2 and when undergoing quench cooling method, these complexities was showed.

Effect of holding time

The effect of holding time only had small influence on the microstructure according to XRD image. The phase ratio was changed with the appearance of the small separation of rhombohedra peaks. Moreover, the sample with longer holding time in 850℃ was more brittle than the shorter holding one, leading to the difficulty of Seebeck and resistivity measurements, and also have worse application future.

4.2 Thermal conductivity Analysis

The thermal conductivities of all the sample were calculated from measured thermal diffusion with the method described in chapter 3.

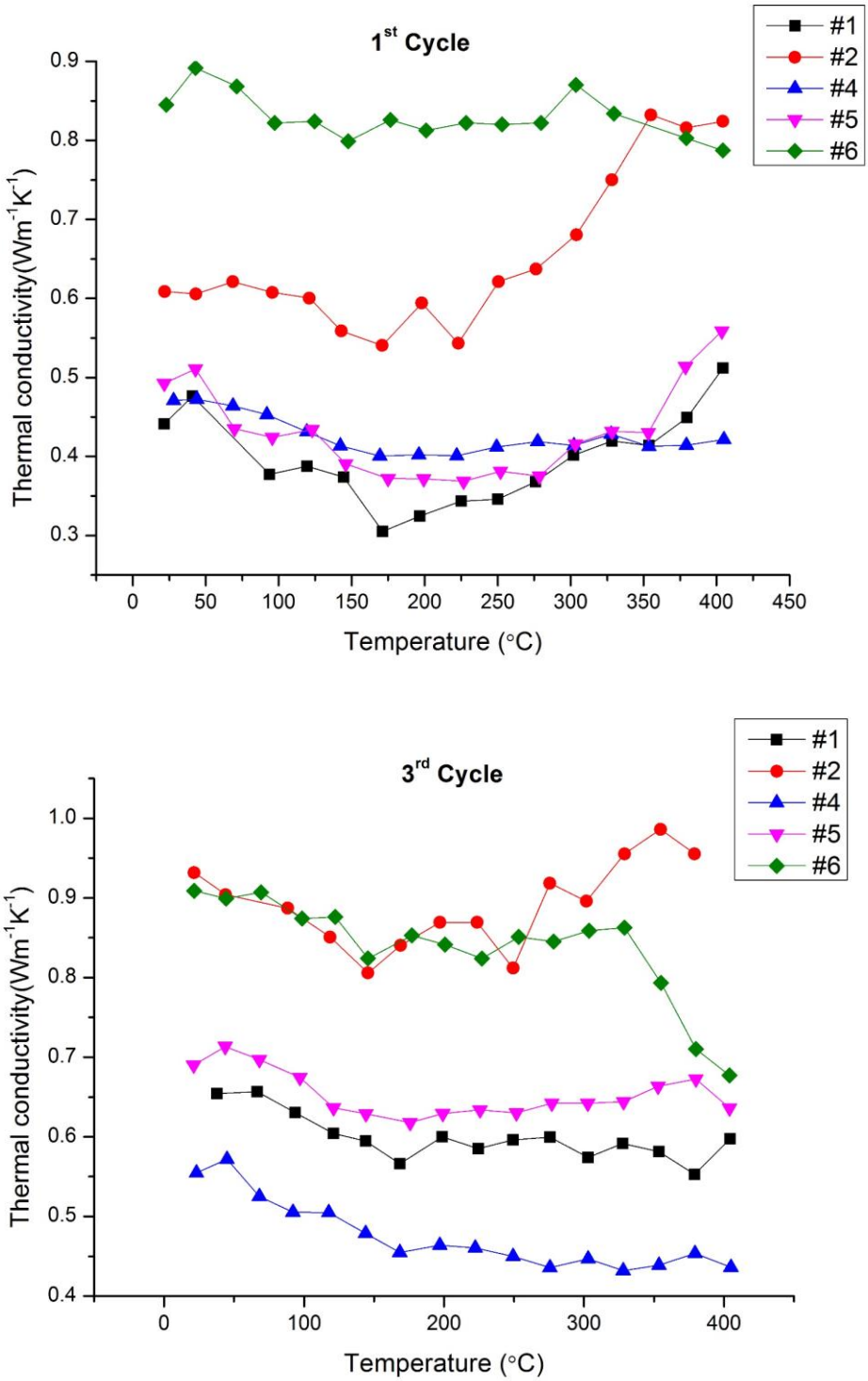

Figure 4.2.1 Thermal conductivity of all the samples for 1st cycle and 3rd cycle

Overall, the thermal conductivities of all the samples were reduced compared to the literature reference. [22] The thermal conductivities of Se substituent PbTe-GeTe materials $Ge_{0.55}Pb_{0.45}Te_{1-x}Se_x$ were reported by Liu in 2016 at temperature windows 300K-700K. The average thermal conductivity of $Ge_{0.55}Pb_{0.45}Te$ was around 2.5 $Wm^{-1}K^{-1}$ without any doping elements. In our experiment, the highest thermal conductivities were 0.9 $Wm^{-1}K^{-1}$ in first cycle (#6) and 1.0 $Wm^{-1}K^{-1}$ in third cycle (#5), still 2 times lower than un-doped $Ge_{0.55}Pb_{0.45}Te$. The lowest value was around 0.3 $Wm^{-1}K^{-1}$ for sample 1, which is comparable to the best reference sample with Se substituent x=0.5.
The decreasing thermal conductivity of the Gd-doped material could be the heavy atom Gd, which acting as point defects and scatter phonons.

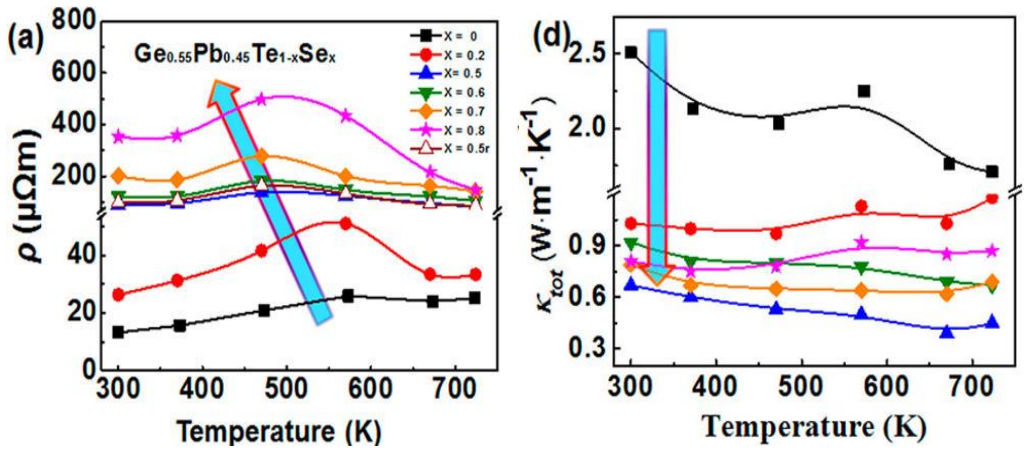

Figure 4.2.2 Resistivity (a) and thermal conductivity (d) for samples $Ge_{0.55}Pb_{0.45}Te_{1-x}Se_x$ with x = 0, 0.2, 0.5, 0.6, 0.7 and 0.8. [22]

Effect of doping with Gd on the cation or anion site

The materials with Gd on anion site had lower thermal conductivity. Since the ratios of doped Gd were the same, the reason could because that exceeded Ge gave more complexities of micro-structures. The lowest thermal conductivity in the first cycle was 0.29 $Wm^{-1}K^{-1}$, obtained from sample 1 at around 170 ℃, which almost reached theoretical lowest thermal conductivity.

Effect of quench versus slow cooling

The thermal conductivities were largely influenced by cooling method according to both first cycle measurement and third cycle measurement.
Compare sample 1 and 4, which have the same chemical composition, sample 1 showed much lower thermal conductivity in the first cycle measurement, but the value increased rapidly after that. The reason might be the slow cooling process of first thermal measurement, which undergo the miscibility gap of phase diagram and caused the change of microstructure, reducing the phase complexities. This phenomenon had less effects on sample 4, because it already went through that range when synthesized.
To verify this hypothesis, an extra XRD for sample 1 after measurement should be performed.

Effect of holding time

The effect of holding time was very small since the values of thermal conductivity for sample 1 and sample 5 were quite similar in all three cycles.

Separation of lattice thermal conductivity and electric thermal conductivity of sample 4

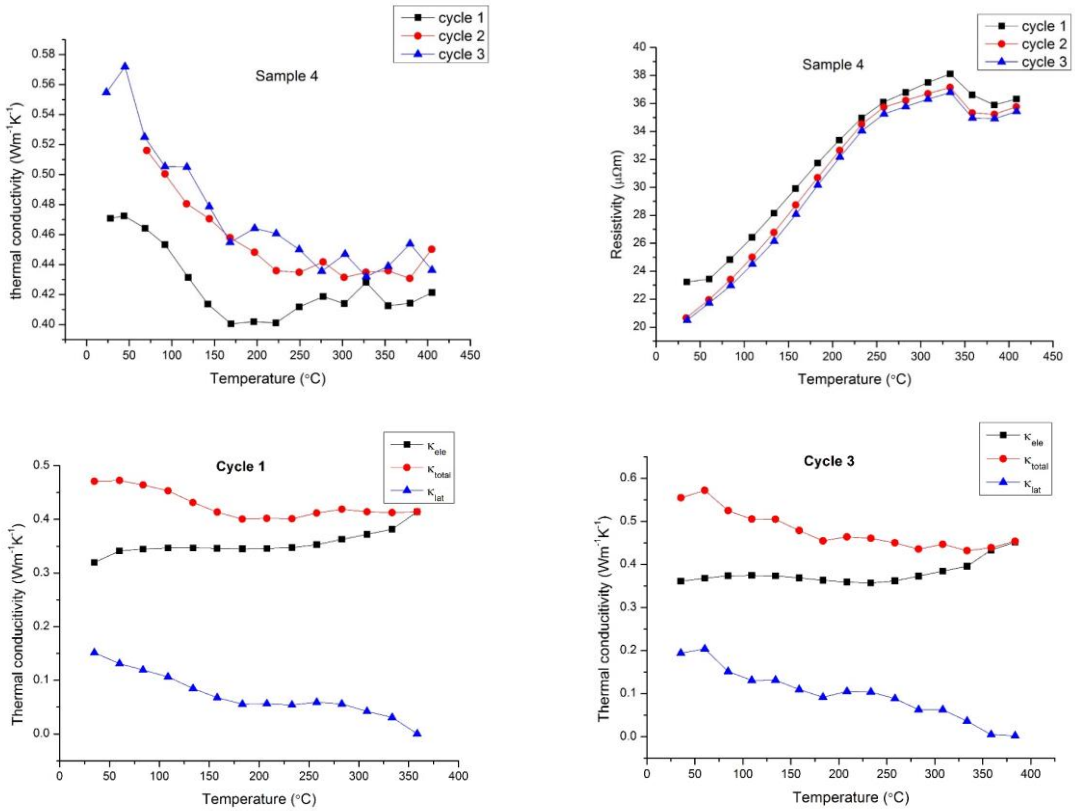

Figure 4.2.3 Thermal conductivity, resistivity and calculated $\kappa_{ele}, \kappa_{lat}$ and κ_{total} of sample 4

The thermal conductivity of sample 4 was different from sample 1, which had the same composition. The trend of three cycles were similar. However, the values of conductivity were similar in 2nd and 3rd cycle at the whole temperature window and only had a small difference compared to sample 4, indicating the thermal property of that material was stable.

To understand the contribution of electron thermal conductivity and lattice thermal conductivity, the resistivity was measured and the κ_e was calculated via the method mentioned in chapter 1.

$$\kappa_e = L\sigma T$$

where L is the Lorentz factor and simply being used as a constant (2.4×10^{-8}).

According to value of the κ_{ele} calculated from resistivity (conductivity) of sample 4, the lattice thermal conductivity of sample 4 declined with the increasing of temperature and only occupied a little of thermal conductivity in the whole temperature range and almost reached zero at 400 degrees. This gave an evidence of the hypothesis that the introducing of heavy atom - Gd, which caused mass disorder and phonons scattering, reduce the lattice thermal conductivity.

4.3 Seebeck and resistivity measurement

The sample 4 was selected to test the Seebeck and resistivity measurement because its lowest thermal conductivity and relatively stable thermal properties.

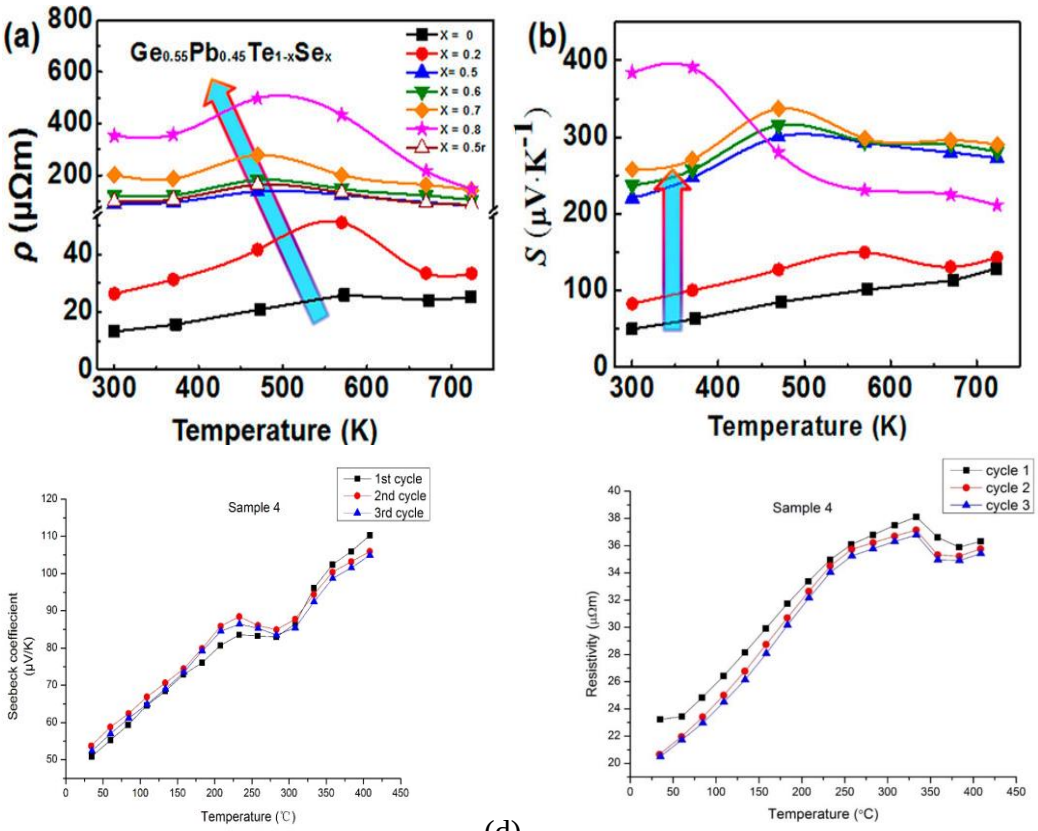

Figure 4.3.1 Resistivity (a) and Seebeck coefficient (b) for samples $Ge_{0.55}Pb_{0.45}Te_{1-x}Se_x$ with x = 0, 0.2, 0.5, 0.6, 0.7 and 0.8. Seebeck coefficient (c) and resistivity (d) of sample 4

Compared to the reference value, where x=0 in figure 4.3.1, the resistivity and seebeck coefficient of sample 4 were quite similar in the whole temperature windows.
So overall speaking, the thermoelectric property of sample 4 was improved compared to the reference paper, with stable and similar Seebeck coefficient, resistivity and reduced thermal conductivity.

Chapter 5. Conclusion

In this bachelor thesis, the $Ge_xPb_{1-x}Te$ based material was doped by 2% gadolinium to improve the thermoelectric properties by reducing thermal conductivity.
The experiments were designed by replacing cation ($Ge_{0.49}Pb_{0.51}Te_{0.98}Gd_{0.02}$) or anion ($Ge_{0.49}Pb_{0.51}Te_{0.98}Gd_{0.02}$) site of $Ge_xPb_{1-x}Te$ with two different methods – directly quench and air-cooling.
The result showed that the material with 2% Gd replacing anion site ($Ge_{0.49}Pb_{0.51}Te_{0.98}Gd_{0.02}$) performed better than the other with both methods, the directly measured thermal conductivity was lower to 0.29 $Wm^{-1}K^{-1}$ for sample 1, which quenched from 850 °C.
However, the stability of sample 4, which obtained from air-cooling method, was best and exhibited the relatively steady and low thermal conductivities (around 0.4 $Wm^{-1}K^{-1}$) for all three cycle.
To see the impact of reaction time, another experiment was made which extend the reaction time to 3 hours for $Ge_{0.49}Pb_{0.51}Te_{0.98}Gd_{0.02}$, the obtained ingot was more brittle than the one with 1 h reaction time. However, the thermal properties of both materials were similar.
The Seebeck coefficient and resistivity were measured on sample 4, which has the lowest and most stable thermal conductivity, which was reduced 2 times compared to early literature reference, indicating that the overall TE property was improved due to the heavy atom mass disorder effects caused by Gd-doping and the microstructure complexities arising from excess Ge in Gd-anion site sample.

Reference

[1] Li, Wen, et al. "Thermoelectric properties of Cu2SnSe4 with intrinsic vacancy." Chemistry of Materials 28.17 (2016): 6227-6232.

[2] Snyder, G. Jeffrey, and Alemayouh H. Snyder. "Figure of merit ZT or a thermoelectric device defined from materials properties." Energy & Environmental Science 10.11 (2017): 2280-2283.

[3] Tritt, Terry M. "Thermoelectric phenomena, materials, and applications." *Annual review of materials research* 41 (2011): 433-448.

[4] Alekseeva, GT, et al. "Donorlike behavior of rare-earth impurities in PbTe." *Semiconductors* 32.7 (1998): 716-719.

[5] Snyder, G. Jeffrey, and Eric S. Toberer. "Complex thermoelectric materials." *Materials For Sustainable Energy: A Collection of Peer-Reviewed Research and Review Articles from Nature Publishing Group*. 2011. 101-110.

[6] Bhandari, CM, and David M. Rowe. "CRC Handbook of thermoelectrics." *CRC Press, Boca Raton, FL* (1995): 49.

[7] Tan, Gangjian, Li-Dong Zhao, and Mercouri G. Kanatzidis. "Rationally designing high-performance bulk thermoelectric materials." *Chemical reviews* 116.19 (2016): 12123-12149.

[8] Pei, Yanzhong, Heng Wang, and G. Jeffrey Snyder. "Band engineering of thermoelectric materials." *Advanced materials*24.46 (2012): 6125-6135.

[9] Zhang, Lijuan, et al. "Lead-free SnTe-based thermoelectrics: Enhancement of thermoelectric performance by doping with Gd/Ag." *Journal of Materials Chemistry A* 4.20 (2016): 7936-7942.

[10] Callaway, Joseph. "Model for thermal thermal conductivity at low temperatures." *Physical Review* 113.4 (1959): 1046.

[11] Callaway, Joseph, and Hans C. von Baeyer. "Effect of point imperfections on thermal thermal conductivity." *Physical Review*120.4 (1960): 1149.

[12] Klemens, PG "Thermal resistance due to point defects at high temperatures." *Physical review* 119.2 (1960): 507.

[13] Abeles, B. "Lattice thermal conductivity of disordered semiconductor alloys at high temperatures." *Physical Review*131.5 (1963): 1906.

[14] Gelbstein, Yaniv, and Joseph Davidow. "Highly efficient functional Ge x Pb 1− x Te based thermoelectric alloys." *Physical Chemistry Chemical Physics* 16.37 (2014): 20120-20126.

[15] Gelbstein, Yaniv, et al. "Controlling metallurgical phase separation reactions of the Ge0. 87Pb0. 13Te alloy for high thermoelectric performance." *Advanced Energy Materials* 3.6 (2013): 815-820.

[16] Wu, Di, et al. "Origin of the high performance in GeTe-based thermoelectric materials upon Bi2Te3 doping." *Journal of the American Chemical Society* 136.32 (2014): 11412-11419.

[17] Rawat, P. K., B. Paul, and P. Banerji. "Lead telluride based thermoelectrics: Approaches for higher efficiency." (2013).

[18] Li, Junqin, et al. "Extremely low thermal conductivity in thermoelectric Ge0. 55Pb0. 45Te solid solutions via Se substitution." *Chemistry of Materials* 28.17 (2016): 6367-6373.

[19] Heremans, Joseph P., Bartlomiej Wiendlocha, and Audrey M. Chamoire. "Resonant levels in bulk thermoelectric semiconductors." *Energy & Environmental Science* 5.2 (2012): 5510-5530.

[20] Pei, Yan-Ling, et al. "High thermoelectric performance realized in a BiCuSeO system by improving carrier mobility through 3D modulation doping." *Journal of the American Chemical Society*136.39 (2014): 13902-13908.

[21] Gorsse, Stéphane, et al. "Microstructure engineering design for thermoelectric materials: an approach to minimize thermal diffusivity." *Chemistry of Materials* 22.3 (2009): 988-993.

[22] Li, Junqin, et al. "Extremely low thermal conductivity in thermoelectric Ge0. 55Pb0. 45Te solid solutions via Se substitution." *Chemistry of Materials* 28.17 (2016): 6367-6373.

[23] Wu, Di, et al. "Origin of the high performance in GeTe-based thermoelectric materials upon Bi2Te3 doping." Journal of the American Chemical Society 136.32 (2014): 11412-11419.